



Wire-EDM performance and surface integrity of Inconel 718 with unique microstructural features fabricated by laser powder bed fusion

Ozkan Gokcekaya^{1,2} · Ali Günen³ · Ferhat Ceritbinmez⁴ · Abdollah Bahador⁵ · Takayoshi Nakano^{1,2} · Melik Çetin⁶

Received: 10 May 2023 / Accepted: 28 December 2023 / Published online: 17 January 2024
© The Author(s) 2024

Abstract

Inconel 718 alloy is difficult to machine using conventional methods due to its physical properties. Thereby, additive manufacturing (AM) of IN718 components with near-net shapes has been extensively studied. Even though AM processes provide shape and size accuracy, there is still the need for the machining of the AM-processed components to achieve the final shape of a component. Laser powder bed fusion (LPBF) has been successfully utilized to fabricate near-net shape IN718 components; moreover, the microstructure of LPBF-IN718 was unique owing to the AM processing, resulting in differences in grain size, grain boundary characteristics, and grain orientations. Furthermore, these microstructural characteristics are expected to alter the machining performance of IN718. Therefore, this study investigated the wire electro-discharge machining (WEDM) performance of LPBF-718 samples compared to wrought IN718 while focusing on the unique microstructure characteristics of LPBF-IN718 samples (lamella, single-crystal, poly-crystal). Three different cutting strategies (rough, semi-finish, and finish) were implemented to understand the performance of the multi-pass cutting phenomenon and its effect on the surface of IN718. For all samples, rough (single pass) cutting displayed high roughness, while finish (three passes) cutting exhibited good surface quality. Compositional analyses on the machined surface showed debris formation including Zn and Cu-containing recast material, indicating wire erosion. The surface of single-crystal LPBF-IN718 after the WEDM process was smooth owing to its large grain size and less amount of grain boundary, resulting in slow cutting speed but a good surface finish. Thus, this study, for the first time, investigated the effect of unique microstructural characteristics of LPBF-fabricated IN718 on WEDM performance and machined surface quality.

Keywords Inconel 718 · LPBF · WEDM · MRR · Surface roughness

1 Introduction

Ni-based superalloys with various alloy compositions have a wide range of industrial applications as cast, wrought, and powder metallurgical forms, particularly in aerospace, automotive, and energy industries, owing to good creep and

fatigue properties with oxidation resistance at high operation temperatures [1–4]. Structural stability at high temperatures and good weldability while preventing defect formation have been achieved with new Ni-based superalloy developments with the realization of fast-cooling techniques of the alloy powders [5]. Moreover, Inconel 718 (IN718) has been

✉ Ozkan Gokcekaya
ozkan@mat.eng.osaka-u.ac.jp

✉ Ali Günen
ali.gunen@iste.edu.tr

¹ Division of Materials and Manufacturing Science, Graduate School of Engineering, Osaka University, 2-1, Yamadaoka, Suita, Osaka 565-0871, Japan

² Anisotropic Design & Additive Manufacturing Research Center, Osaka University, 2-1, Yamadaoka, Suita, Osaka 565-0871, Japan

³ Faculty of Engineering and Natural Sciences, Department of Metallurgy and Materials Engineering, Iskenderun Technical University, Iskenderun, Hatay 31200, Turkey

⁴ Manufacturing-Research and Development, Haier Group, Eskişehir 26010, Turkey

⁵ Razak Faculty of Technology and Informatics, Universiti Teknologi Malaysia, Jalan Sultan Yahya Petra, 54100 Kuala Lumpur, Malaysia

⁶ Department of Manufacturing Engineering, Faculty of Technology, Karabuk University, Karabuk, Turkey

widely preferred for engine components, nuclear reactors, and combustor applications owing to its high-temperature strength and corrosion resistance at high operating temperatures [6].

Recently, laser-based additive manufacturing (AM) methods have been widely used to fabricate complex geometries with near full density from 3D CAD models, thus allowing design freedom while avoiding material waste [7]. Due to the advantages of AM methods, laser powder bed fusion (LPBF) has been applied to produce near-final shape IN718 alloy parts [1]. The LPBF offers tunable microstructure with the control of process parameters [8, 9], improving the hardness, yield, and ultimate strength of IN718, exhibiting comparable or even better performance than forged or cast IN718 alloy [10]. Moreover, the LPBF process is capable of forming unique crystallographic textures in IN718 owing to epitaxial growth, realizing anisotropy in mechanical strength [11]. Besides, in a recent study, the formation of the single-crystal-like, lamella, and poly-crystal microstructure in IN718 has been reported with the variation time of LPBF process parameters [8], resulting in strengthening via texture effect.

Even though the parts fabricated by LPBF are near-net shape [12], they still require post-process machining for critical industrial applications. Besides, most of the machining processes apply significant heat, vibration, chemical reaction, and/or electrochemical energy on the surface, which can be detrimental to the performance of the component. Therefore, electric discharge machining, which is a non-contact machining process, has been widely employed for the precise processing of final components for aerospace, defense, and automotive applications [13, 14]. Wire electro-discharge machining (WEDM) has been widely used for the machining of electrically conductive materials as a cost-efficient and optimum machining process in terms of its non-contact cutting with cooling media resulting in minimal thermal effect and no mechanical cutting force on the surface of the product compared to conventional machining processes [15, 16]. As a result, WEDM has been accepted as a primary machining technique for various industrial applications.

However, the limitations of the WEDM process are the machining time compared to other processes and the surface finish of the final product [17, 18]. Many studies have been conducted to optimize the process parameters of WEDM in terms of material removal rate (MRR), roughness, eroded residuals, etc. [15, 19–22]. However, there is still a lack of understanding of the effect of microstructural features of additively manufactured IN718, including crystallographic orientation, grain size, and grain boundary, on WEDM performance and machined surface properties. The previous key studies focusing on

WEDM cutting of Inconel groups, which are in the class of alloys that are difficult to machine, are briefly summarized below.

Ramakrishnan and Karunamoorthy [23] used artificial neural network analysis to find the best parameters and evaluate the effect of each parameter on the quality of the machined surface to cut Inconel 718 material by the WEDM method, reporting that all input parameters used in the study affected the processing quality at different rates. Dabade and Thejasree [24, 25] experimented with machining IN718 by WEDM in separate studies considering the variation of process parameters while considering MRR, surface finish, and kerf width by Taguchi technique. They reported that an increase in discharge current increases surface roughness. Dhale and Deshmukh [26] investigated the cutting of Inconel 718 alloy with wire electrodes of different thicknesses in the WEDM method and investigated the effect of electrode wire thickness on dimensional deviation, wire consumption, and surface quality. They found that with the decrease in wire electrode diameter, cutting precision increased, and wire and workpiece waste decreased, resulting in lower environmental impacts, reduction in craters on the machined surfaces, reduction in microhardness change, and reduction in recast layer thickness value. Karataş [27] machined Inconel 718 alloy via the WEDM method, considering changes in MRR and kerf by process parameters using gray relational analysis (GRA) and analysis of variance (ANOVA) methods. It was concluded that wire tension significantly affected the MRR while the effect of dielectric fluid pressure was insignificant.

When the published studies in the literature are examined, it has been determined that the cutting of additive manufacturing Inconel alloys, which are replacing wrought Inconel alloys day by day, with WEDM has not been systematically studied yet. Therefore, this study has been planned to provide valuable information for the WEDM process of additively manufactured metal materials.

Moreover, in addition to WEDM cutting parameters, the repetition of cutting passes also affects the surface integrity seriously due to the difference in MRR for each cutting pass. Considering published studies, there has been no report discussing the effect of the unique microstructure of the IN718 fabricated by LPBF on cutting speed, MRR, and surface integrity. LPBF method which is a fast-cooling process induced continuous grain growth from the previously solidified layer to the subsequent layer, thus promoting columnar grains with crystallographic texture control, such as strong $\langle 100 \rangle$ texture in terms of printing metal materials with cubic crystal lattice due to (100) preferred epitaxial growth [28–30]. Furthermore, the crystallographic texture of IN718 fabricated by LPBF varied

depending on process parameters, with microstructures of $\langle 100 \rangle / \langle 110 \rangle$ lamella, $\langle 100 \rangle$ single-crystal-like, and randomly oriented poly-crystal-like being produced depending on the applied laser energy density. The relation between grain orientation and finished surface roughness after micromachining and orthogonal cutting of cp-Ti has been recently reported by Kieren-Ehse et al. [31], showing the correlation between grain orientation and machining performance as well as surface roughness, thus highlighting the importance of crystallographic orientation control via LPBF and its effect on WEDM performance as discussed in this study.

Therefore, this study investigated the effect of IN718 fabricated by LPBF with different microstructural characteristics considering grain orientation, grain size, and grain boundary on its WEDM performance and its comparison with wrought IN718. For this purpose, three different WEDM processes were implemented, which were rough cut, semi-finish cut, and finish cut to process LPBF-fabricated IN718. Since most failures such as fatigue, corrosion, and wear are sensitive to the surface quality of the material, this study presented an understanding of WEDM performance on different surface characteristics that are highly important in order to increase the service life of IN718 parts.

2 Materials and methods

2.1 Fabrication of IN718 by LPBF

IN718 samples were fabricated by LPBF (EOS M290), using gas-atomized IN718 powder exhibiting the same chemical composition as the wrought IN718 (Table 1) while containing visible satellites ($D_{50} = 32.3 \mu\text{m}$), as shown in Fig. 1a, although representing good powder quality for LPBF [32]. The fabrications were carried out at $80 \text{ }^\circ\text{C}$ base temperature to prevent disturbance of temperature fluctuations. The LPBF process was performed in a high-purity argon gas atmosphere to avoid *in-situ* oxidation.

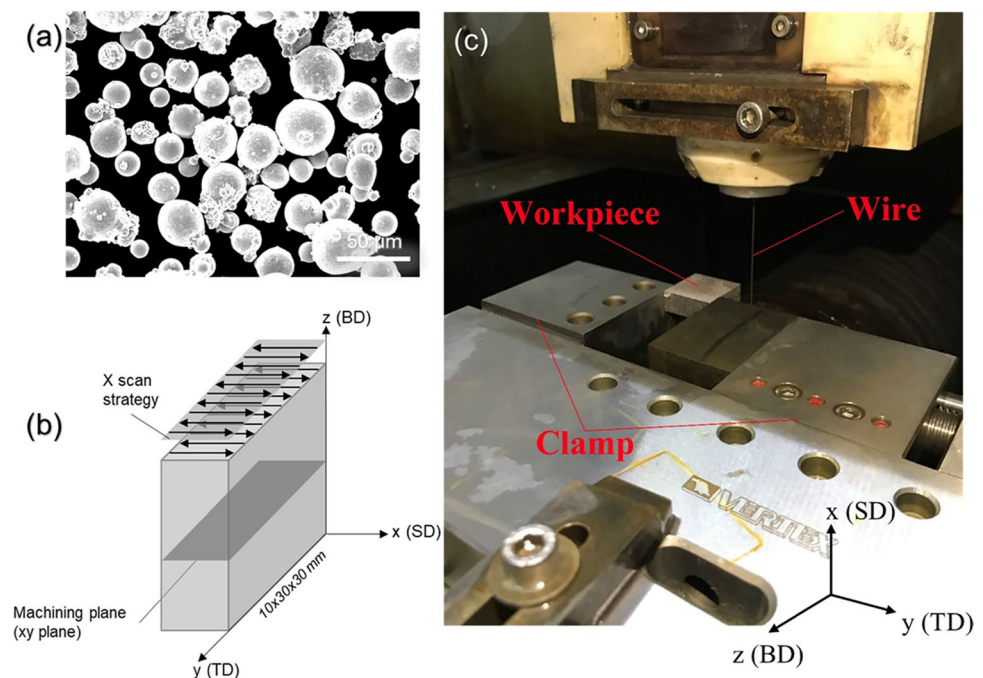
A bidirectional scan strategy (X scan) was applied to fabricate $10 \times 10 \times 30 \text{ mm}$ samples for WEDM experiments (as illustrated in Fig. 1b), which promoted unique crystallographic orientations with changing process parameters [28–30].

To develop crystallographic texture, LPBF laser power ($P = 180 \text{ W}, 360 \text{ W}$) and scan speed ($V = 1000 \text{ mm/s}, 1400 \text{ mm/s}$) varied while powder layer thickness ($h = 0.040 \text{ mm}$) and hatch space ($d = 0.080 \text{ mm}$) was fixed [8]. According to these process parameters, the laser energy density (E) of the LPBF-fabricated IN718 samples,

Table 1 Chemical composition of IN718 for powder used in LPBF and wrought material

	Ni	Cr	Nb	Mo	Ti	Al	Co	Cu	C	Si	Mn	P	S	B	Fe
Min	50	17	4.75	2.8	0.65	0.2									
Max	55	21	5.5	3.3	1.15	0.8	1.0	0.3	0.08	0.35	0.35	0.015	0.015	0.006	bal

Fig. 1 SEM image of (a) IN718 powder; (b) schematic presentation of X scan strategy and LPBF build size with the setting of (c) LPBF-IN718 sample on WEDM apparatus to cut along xy plane



calculated by $E = \frac{P}{V \times h \times d}$, was in the descending order as $E_{\text{LPBF-1}} > E_{\text{LPBF-2}} > E_{\text{LPBF-3}}$, in which notations, process parameters, and microstructure characteristics of the LPBF-718 samples are given as follows:

$P = 360$ W and $V = 1000$ mm/s (LPBF – 1, lamella texture)

$P = 360$ W and $V = 1400$ mm/s (LPBF – 2, single – crystal – like texture)

$P = 180$ W and $V = 1400$ mm/s (LPBF – 3, poly – crystal texture)

The wrought IN718 were subjected to a heat treatment process where they were heated from 980 to 1095 °C for 1 h and then rapidly cooled by immersing them in water until they reached room temperature. Afterward, the samples underwent a two-step aging treatment. In the first step, they were held at 720 °C for 8 h and then slowly cooled in a furnace to 620 °C at a rate of 50 °C per hour. In the second step, they were held at 620 °C for another 8 h and then allowed to cool naturally in the surrounding air until they reached room temperature.

2.2 Machining methods

The IN718 specimens were cut by WEDM to observe the effect of machining on the perpendicular surface (xy plane) to the build direction (BD). In this study, four different Inconel 718 materials were cut by connecting to the “Charmilles Robofil 290P” WEDM workbench using a vertex precision vice and combined supported perforated flat shoes as shown in Fig. 1. “Bedra topas plus X” brand zinc-rich brass-coated 0.25-mm-thick copper wire was used as the wire electrode material. Pure water was used as the dielectric fluid for the evacuation of the abraded workpiece and wire electrode residues from the environment [33]. The dielectric liquid was sprayed from the upper and lower nozzles in the inlet and outlet areas.

WEDM was performed to obtain three types of surface finish, which are roughing with a single pass of cutting wire, semi-finish, and finish with two and three passes of wire cut,

respectively [34]. Parameters of WEDM used in this study are given in detail in Table 2.

2.3 WEDM performance

WEDM was applied to three types of IN718 products with different microstructures produced by LPBF and a wrought standard IN718 purchased from Acciaierie Valbruna (Italy). The cutting speed and material removal rate (MRR) with upper and lower nozzle pressure values obtained after cutting processes using different cutting regimes are given in Table 4. Considering Table 4, the MRR is high and the cutting speed is low in rough cutting because there is a risk of the wire breaking in rough cuts [22]. On the other hand, MRR is low and cutting speed is high in finishing cuts since only 5 μm is removed from the material surface. Upper and lower nozzle pressure values are set to zero in order to increase wire stability and improve cutting quality in the finish-cutting processes. The surface roughness of the samples after WEDM cutting was determined by using a Profilm 3D profilometer (Filmetric, USA) at a speed of 0.1 mm/s and scanning an area of 1 mm².

2.4 Characterization

The XRD studies were carried out to confirm the texture formation in as-built IN718 samples according to the exemplary study [8] by utilizing Malvern Panalytical EMPYREAN operated at 60 kV and 60 mA with CuKα radiation in scan range from 10 to 100° and scan rate 1°/min. The density measurements were carried out by Archimedes’ method (LA310S, 147 Sartorius, Germany). Microstructural characteristics of as-built IN718 and WEDM-processed IN718 samples were investigated by field-emission scanning electron microscopy (FE-SEM; JSM-6500, JEOL, Japan) with

Table 2 Machining parameters used in the WEDM

Cutting mode	Roughing	Semi-finishing		Finishing		
		1st	2nd	1st	2nd	3rd
Pass	1st	1st	2nd	1st	2nd	3rd
Gap voltage (V)	80	80	120	80	120	120
Pulse on time (μs)	1	1	2	1	2	2
Pulse off time (μs)	21	21	23	21	23	23
Wire speed (m/min)	12	12	8	10	8	8
Discharge current (A)	40	40	99	48	99	99
Wire tension (kg)	1,1	1,1	1,6	1,2	1,6	1,6
Feed rate (mm/min)	75	75	100	100	100	100
Wire-offset (μm)	0	40	0	40	5	0

an electron backscatter diffraction (EBSD) and energy dispersive spectroscopy (EDS) systems (NordlysMax3, Oxford Instruments, UK). The measurements were performed with a 2- μm step size at 20 kV operating voltage. Data curation for microstructural features, such as grain orientation map (inverse pole figures, IPF), crystallographic texture strength (multiples of uniform distribution, MUD), and mapping of high-angle grain boundaries (HAGBs), was performed by HKL Channel 5 software (Oxford Instruments, Cambridge, UK). The quantitative analyses of HAGBs were given by HAGB length per area ($\mu\text{m}/\mu\text{m}^2$) collected from EBSD measurements.

3 Results and discussion

XRD patterns and SEM microstructure images of wrought and LPBF-IN718 samples are presented in Figs. 2 and 3, respectively. According to the XRD patterns, both the wrought and LPBF samples exhibited solely the FCC Cr-Ni-Fe structure (ICDD Card No: 00–031–0619) with no other phase formation or precipitation. However, the most dominant peak of the wrought-IN718 was the (111) peak at 43.66 degrees, whereas the highest intensity peak in the

LPBF sample was indicated to be the (200) peak at 50.65 degrees. Owing to the epitaxial growth during layer-by-layer fabrication of the LPBF process, IN718 grains grew along (100) preferential growth directions and the LPBF process promoted (100) dominant grains with unique microstructural characteristics depending on laser energy density [8].

The detailed microstructural analyses were presented in Fig. 4, and quantitative data was included in Table 3. While LPBF powders showed random (mix) orientation, low energy density fabrication (LPBF-3) also varied in grain orientation (mix of (200), (111), and (220)). However, with the increase in laser energy density, the microstructure of LPBF-2 exhibited only (200) oriented grains, indicating a single-crystal-like microstructure. Further increase in laser energy density (LPBF-1) demonstrated major (200) and minor (220) grain formation, indicating (100)/(110) lamella-oriented microstructure. The reason for different microstructure formation with the change in laser energy density was attributed to the melt pool size and shape, as explained in detail in our previous report and supported by the literature studies [8, 35–37]. The well-established control over the microstructure of LPBF-IN718 with laser energy density resulted in variations in grain size and the HAGB length per area. While the LPBF-3 sample had an average grain size of 12.64 μm , with the increase in laser energy density, the grain size of LPBF-2 and LPBF-1 increased to 20.58 μm and 21.34 μm , respectively (Table 3). Note that the electrical and thermal conductivities of the material, which affect machinability, are altered by the grain size, grain boundary, and grain orientation; thus, the microstructural characteristics of the samples are critical for determining the machining performance [31, 38–41].

Considering SEM observations of wrought and as-built samples, the wrought IN718 sample has a homogeneous microstructure appearance, while LPBF-IN718 samples have a microstructure appearance reminiscent of dendritic and interdendritic structures. It has been reported in the literature that the direction of dendritic growth depends on the direction of heat flow and is mostly perpendicular to the substrate material due to a steep thermal gradient along the build direction [1]. However, as seen in the EDS analyses in Fig. 3 taken over a dendritic and interdendritic structure on the SEM microstructure view, the chemical compositions of the dendritic and interdendritic regions of the LPBF-IN718 samples were found to be close to each other owing to the high cooling rate of LPBF process limiting the segregation and resulting similar elemental distribution to the wrought IN718. Considering the grain size of wrought (6.5 μm), LPBF-IN718 samples consisted of larger grains (12.64–21.34 μm) due to epitaxial growth [42].

Figures 5, 6, 7, and 8 show the SEM views and EDS point analyses of the rough, semi-finish, and finish cut surfaces of four different IN718 samples exposed to high

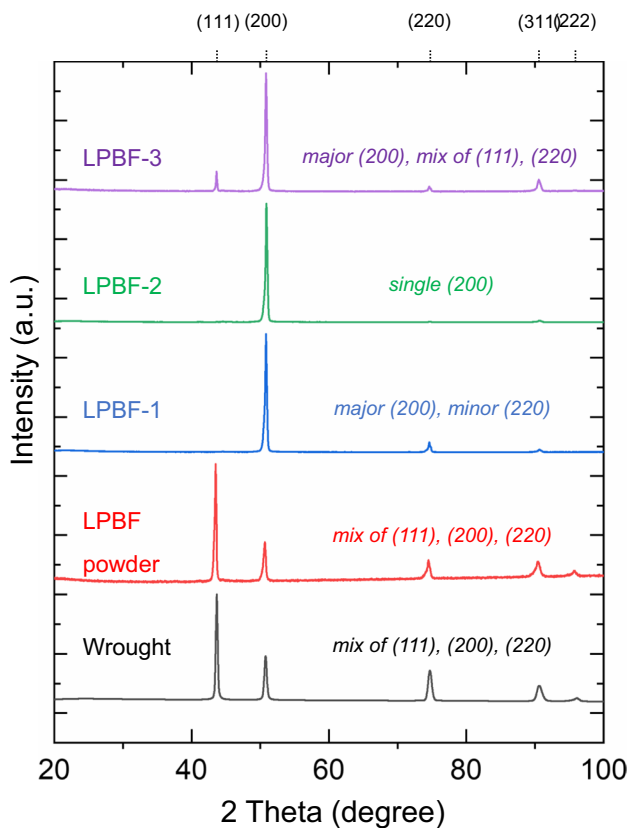


Fig. 2 XRD patterns of wrought and LPBF-fabricated IN718 samples with variation of laser energy-induced grain orientations

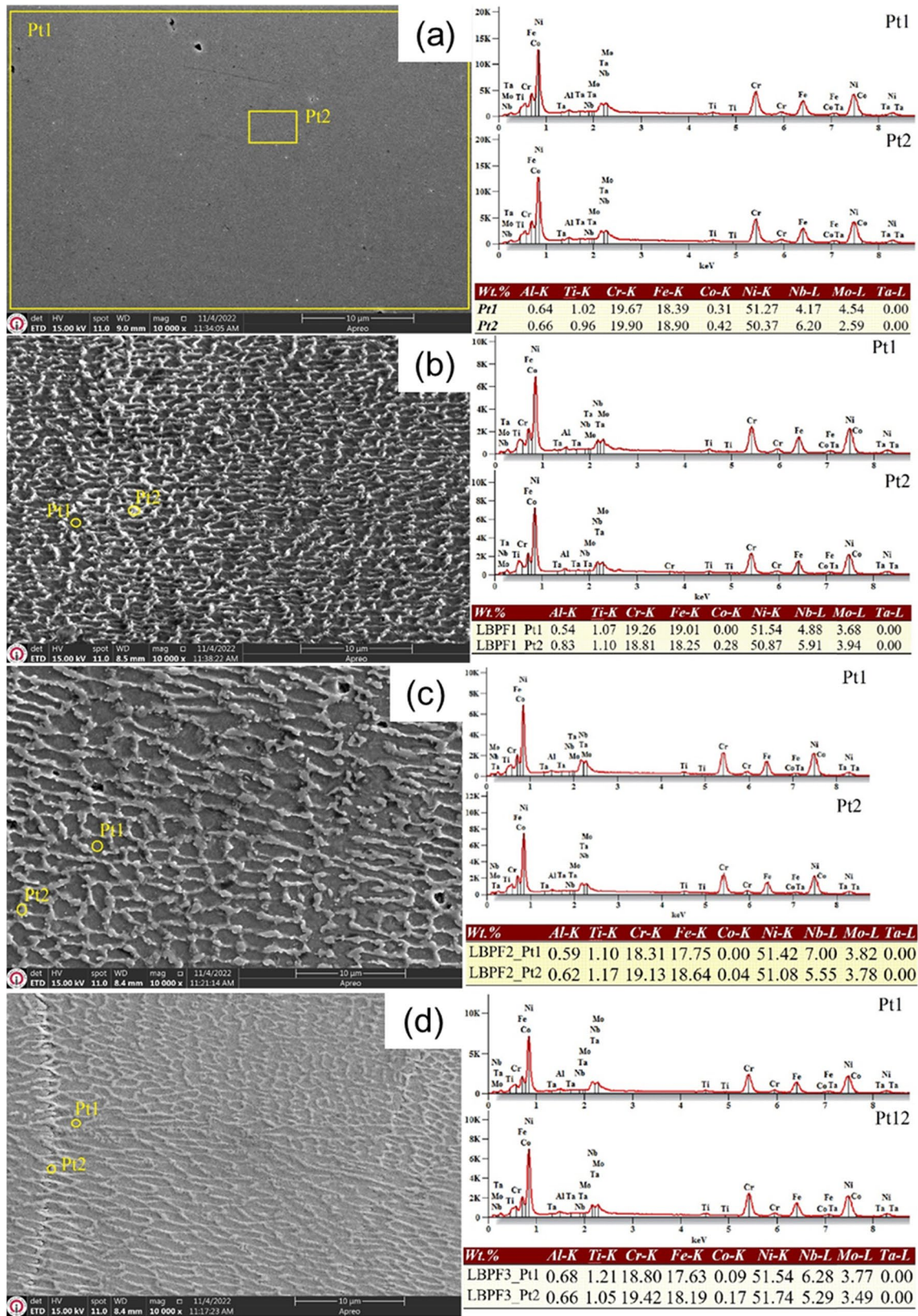


Fig. 3 SEM and EDS analysis of IN718 used in experimental studies: (a) wrought, (b) LBPf-1, (c) LBPf-2, and (d) LBPf-3

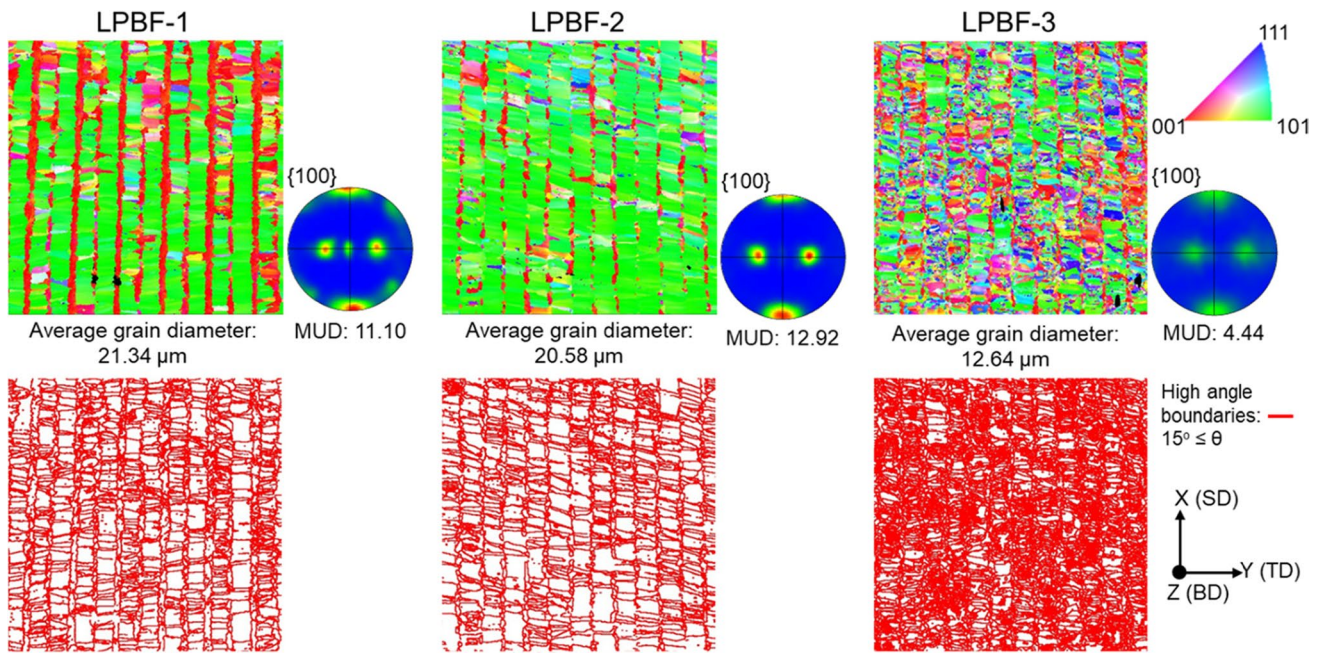


Fig. 4 IPF maps, {100} pole figures, and HAGB maps showing the variation in grain orientation, average grain size, and HAGB distribution

Table 3 Characteristics of wrought and LPBF-fabricated IN718 with unique microstructural features

Sample (IN718)	Density (g/cm ³)	HAGB length per area (μm/μm ²)	Grain size (μm)	Electrical resistance at XY plane (Ω)	Texture characteristics
LPBF-1 (E=112.5 J/mm ³)	8.22	0.056	21.34	2.42 × 10 ⁻⁵	Bi-crystal Major {100} and minor {110}
LPBF-2 (E=80.4 J/mm ³)	8.22	0.053	20.58	2.02 × 10 ⁻⁵	Single-crystal {100}
LPBF-3 (E=40.2 J/mm ³)	8.20	0.117	12.64	2.32 × 10 ⁻⁵	Poly-crystal Major {100} and mix of {110} and {111}
Wrought	8.19	-	6.5	2.55 × 10 ⁻⁵	Poly-crystal Mix of {111}, {100}, and {110}

IN718 theoretical density = 8.19~8.22 g/cm³

discharge energy during the WEDM process. WEDM is a thermal process for removing unwanted material via eroding based on the formation of intense sparks generating high temperatures reaching over the melting point of the material [43, 44]. For a successful application of WEDM, the electrical, thermal conductivity, specific heat capacity, and thermal expansion properties of the machined material play a critical role in obtaining a good surface finish [45]. Moreover, the grain boundaries and segregations in the material can alter these material properties [46, 47]. The surface morphology of all machined samples in this study looked similar, revealing the presence of globules, craters, and debris. However, the microstructural characteristics of LPBF-IN718 and wrought samples showed significant differences, which influenced the WEDM performance

(MRR, cutting speed) and quality of the machined surface (residuals, roughness).

With the increase in the number of cutting passes from rough (one pass) to finish cut (three passes), the debris and globules on the surface of each sample decreased notably (Figs. 5, 6, 7, and 8a–c). This phenomenon correlated with EDS analyses recorded on the surface of each sample. The compositional analyses on the machined surface of wrought IN718 detected the existence of Cu and Zn in the range of 17.20–36.62 wt.% and 7.68–14.24 wt.%, respectively (Fig. 5a), indicating the existence of recast material formed on the surface due to the erosion of brass-coated Cu wire.

The amount of recast material on each sample surface decreased with semi-finish and further decreased with finish cut, as well as corresponding to the decrease

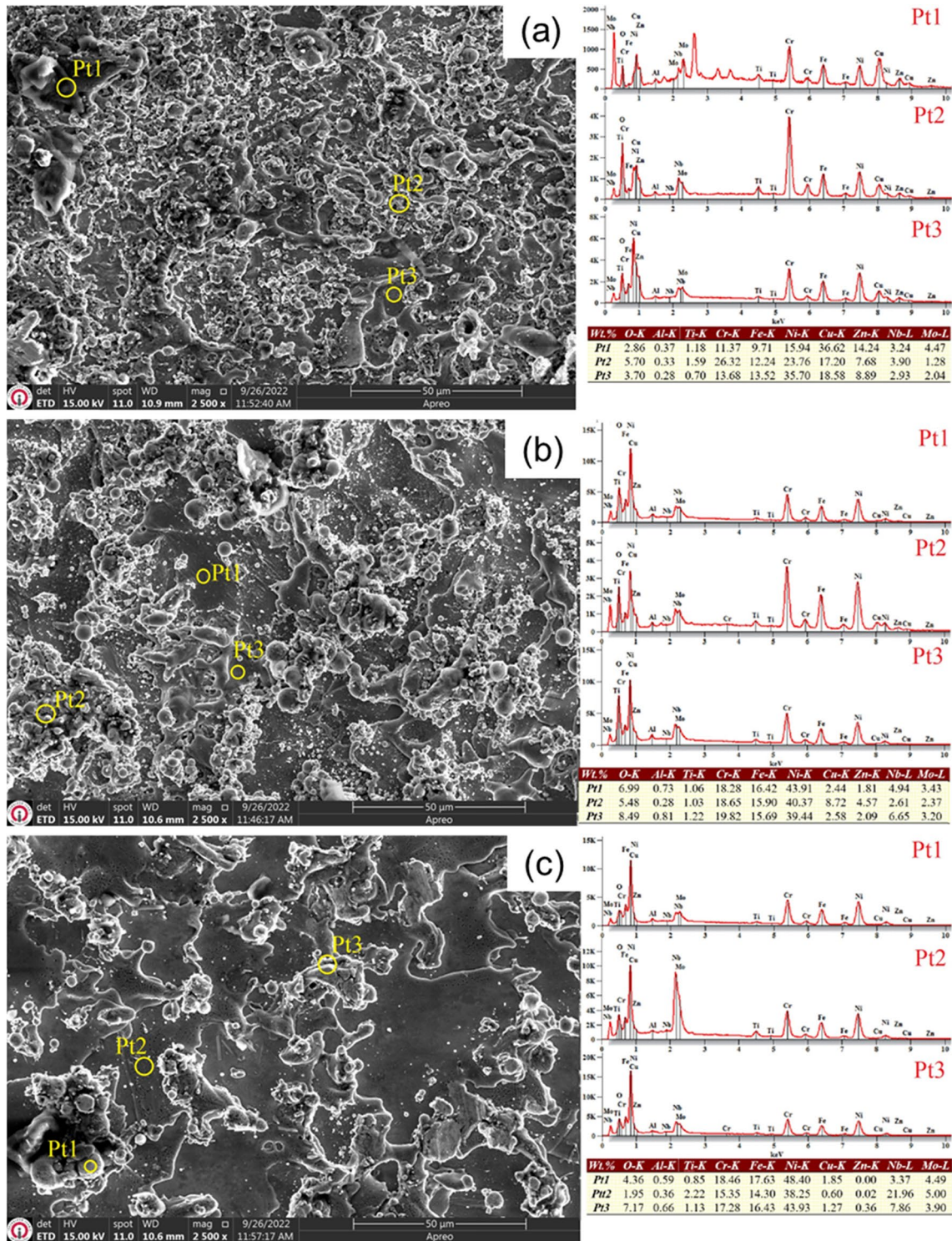


Fig. 5 SEM and EDX analysis of wrought after (a) rough, (b) semi-finish, and (c) finish cut

in MRR value (Table 4). However, it is noteworthy to mention that the debris and globules were less on the LPBF-IN718 samples compared to wrought samples, especially after rough cutting, which was also identified

by EDS analyses resulting in low Cu and Zn contamination (Figs. 5, 6, 7, and 8a). The less debris formation is attributed to the lower amount of grain boundary in LPBF samples owing to larger grains, possibly resulting

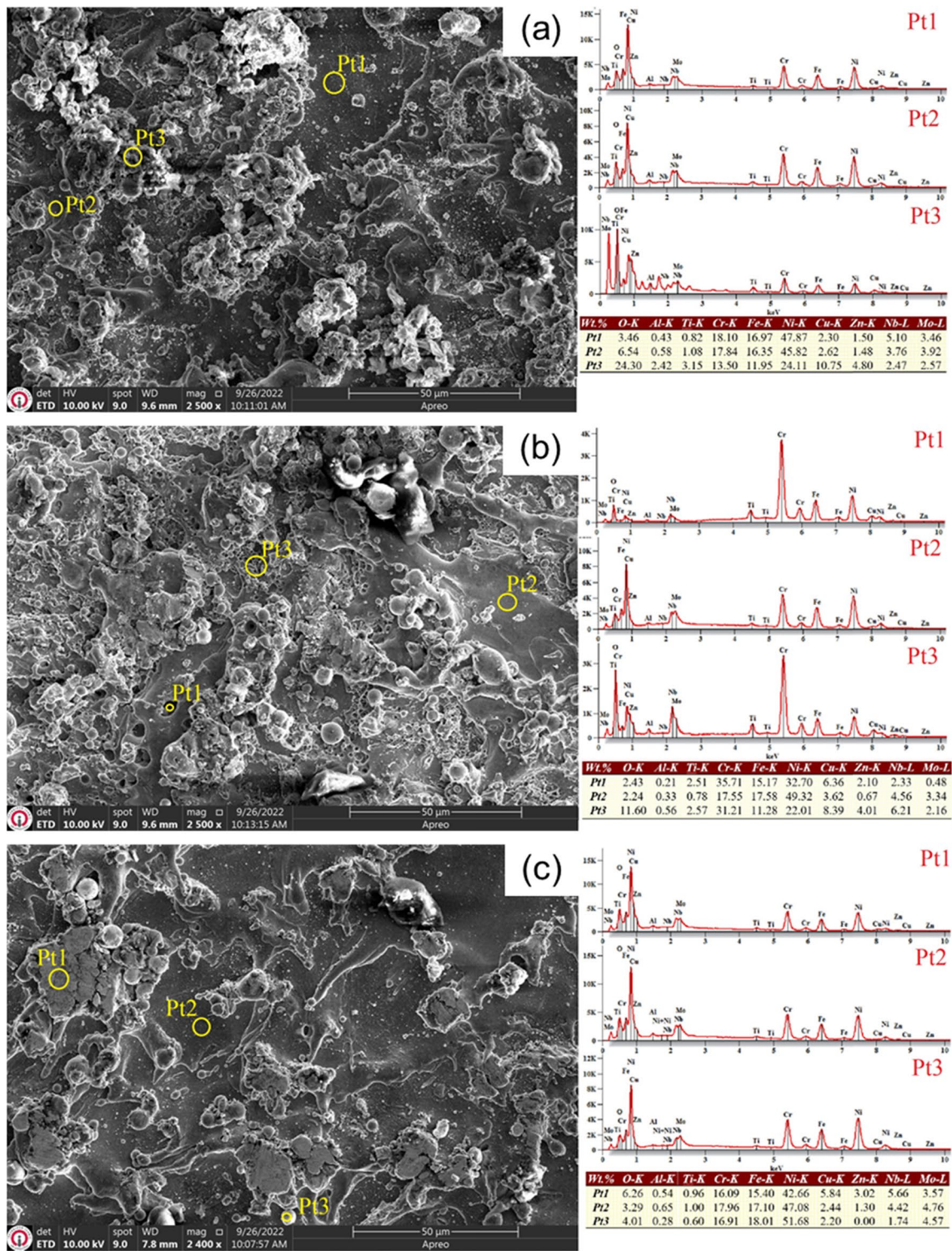


Fig. 6 SEM and EDX analysis of LPBF-1 after (a) rough, (b) semi-finish, and (c) finish cut

in less fluctuation in discharge pulse during the WEDM process.

The surface roughness distribution on wrought and LPBF samples after rough, semi-finish, and finish cuts

was observed by a 3D profilometer, and the findings were reported in Fig. 9, besides the overall machining performance (surface roughness, cutting speed, and MRR) of IN718 was summarized in Fig. 10. The surface morphology

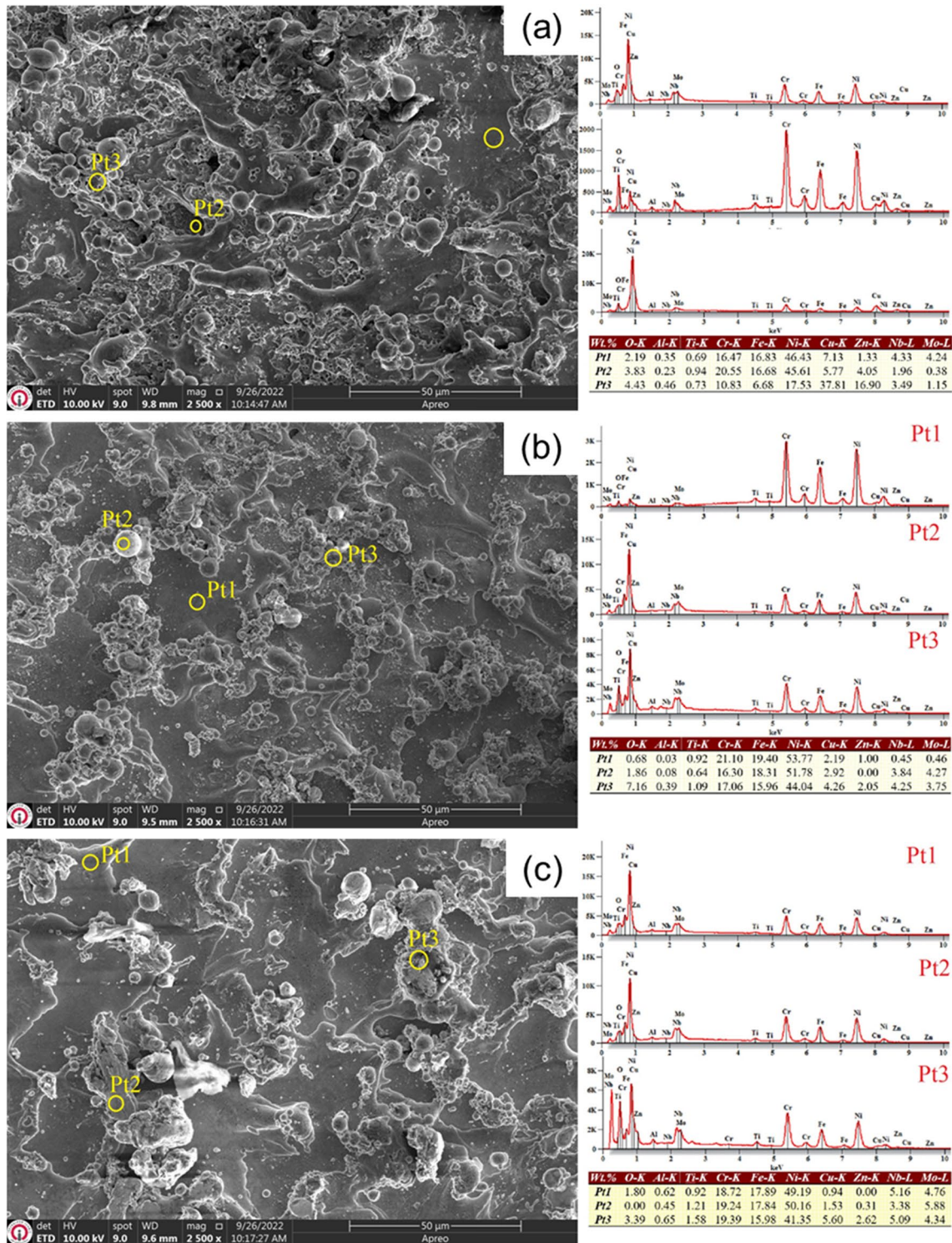


Fig. 7 SEM and EDX analysis of LPBF-2 after (a) rough, (b) semi-finish, and (c) finish cut

after WEDM is irregular compared to the machined surfaces by conventional methods. The WEDM surface was not created by contact with the cutting tool, but rather formed by irregular craters [48], such as recast material and remelted

IN718 [49], as a result of the eroding process reaching over melting temperature of the IN718 sample and brass-coated Cu wire. Moreover, the amount of debris on the machined surface correlates with the thickness of the machined surface

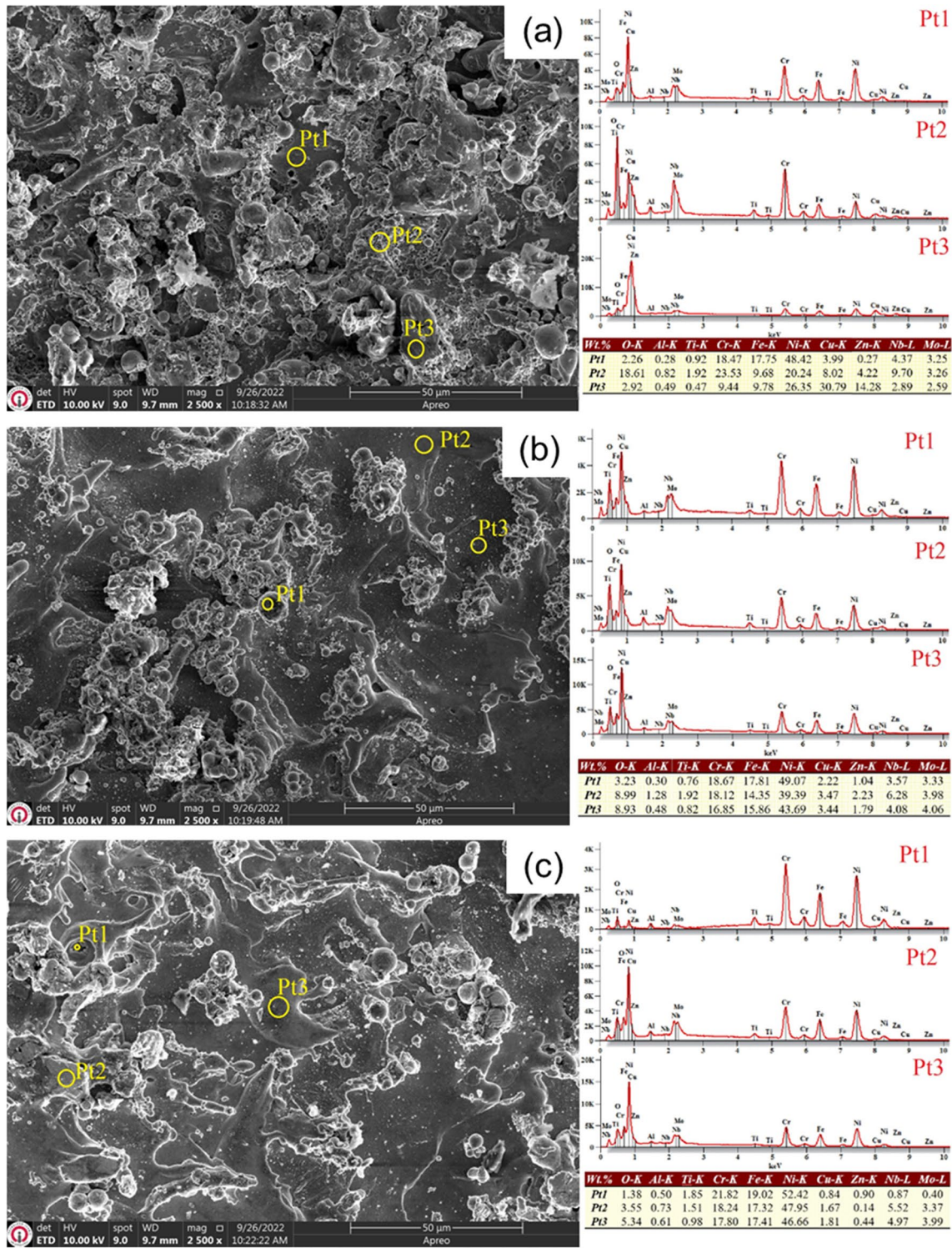


Fig. 8 SEM and EDX analysis of LPBF-3 after (a) rough, (b) semi-finish, and (c) finish cut

layer [50]. Therefore, the surface roughness of each sample was the highest after the rough cut and lowest after the finish cut, which correlated with the MRR value, indicating that the high MRR during the rough cut eroded the brass-coated

Cu wire significantly and formed a high amount of recast material on the surface. However, the finish cut performed with 3 passes showed a low MRR value and allowed the removal of the residues via dielectric fluid.

Table 4 WEDM performance of IN718 depending on machining parameters

Inconel 718	Cutting mode	Pass	Cutting speed (mm/min)	Material removal rate (MRR, mm ³ /min)	Upper nozzle pressure (bar)	Lower nozzle pressure (bar)
Wrought (poly-crystal)	Roughing	1	5.20	23.64	3.40	6.20
		2	16.10	18.02	0.00	0.00
	Semi-finishing	1	5.40	24.18	3.40	6.10
		2	20.60	12.29	0.00	0.00
		3	22.70	1.74	0.00	0.00
	LPBF-1 (lamella)	Roughing	1	4.50	20.43	3.70
2			21.80	13.15	0.00	0.00
Semi-finishing		1	4.50	20.36	0.00	0.00
		2	22.50	13.36	0.00	0.00
		3	22.60	1.68	0.00	0.00
LPBF-2 (single-crystal)		Roughing	1	3.50	15.91	3.50
	2		16.47	9.97	0.00	0.00
	Semi-finishing	1	3.40	15.44	3.50	6.10
		2	17.10	10.49	0.00	0.00
		3	22.60	1.73	0.00	0.00
	LPBF-3 (poly-crystal)	Roughing	1	4.20	18.81	3.50
2			19.80	11.52	0.00	0.00
Semi-finishing		1	4.10	17.90	1.50	4.20
		2	21.40	12.55	0.00	0.00
		3	22.60	1.66	0.00	0.00

The main consideration for the machining performance of IN718 samples in this study was the effect of highly oriented big grains due to the strong thermal gradient of the LPBF process forming (100) epitaxial growth [8]. It has been reported that microstructural characteristics can be tuned with the formation of crystallographic texture, resulting in grain growth along multiple build layers and fewer grain boundaries [32]. In this study, LPBF-3 showed poly-crystal microstructure, resulting in a smaller grain size and more HAGB length per area compared to LPBF-1 and LPBF-2 with strong crystallographic orientation. These microstructural characteristics of LPBF-3 influenced its machining performance, exhibiting higher surface roughness even after the finish cut compared to other LPBF-IN718 samples (Fig. 9).

It has been reported that the thermal and electrical conductivity of poly-crystal materials were influenced by the amount of existing grain boundaries (as referring to grain size) composed of defects and impurities [38]. Therefore, grain boundaries are easier to be eroded by discharge pulse compared to the grain. LPBF-IN718 samples with larger grain than wrought consisted of 0.056 $\mu\text{m}/\mu\text{m}^2$, 0.053 $\mu\text{m}/\mu\text{m}^2$, and 0.117 $\mu\text{m}/\mu\text{m}^2$ HAGB length per area for LPBF-1, LPBF-2, and LPBF-3, respectively. This indicates that

LPBF-IN718 samples with large grains and less grain boundary require more machining time, thus resulting in lower MRR and slow cutting speed, as shown in Table 4 and Fig. 10. Intriguingly, LPBF-1 exhibited relatively high cutting speed and MRR compared to LPBF-3 which had smaller grains and more grain boundaries. It can be assumed that LPBF-1 samples fabricated with higher laser energy density than LPBF-3 retained more residual stress due to the formation of a bigger melt pool during the LPBF process. Residual stress can result in misorientation inside a grain and form dislocations which act like a grain boundary and possibly increase the removal rate of IN718. However, this prediction requires further observations, thus planned as a future study.

In this study, LPBF-2 with (100) single-crystal-like microstructure exhibited low MRR, slow cutting speed, and comparably less surface roughness after the WEDM process (Fig. 10). These results were mainly attributed to bigger grain size and less grain boundary. However, it has been reported that crystallographic orientation control for LPBF-fabricated samples can enhance the structural and functional properties of materials [8, 9, 51]. Besides, the influence of crystallographic anisotropy on the WEDM

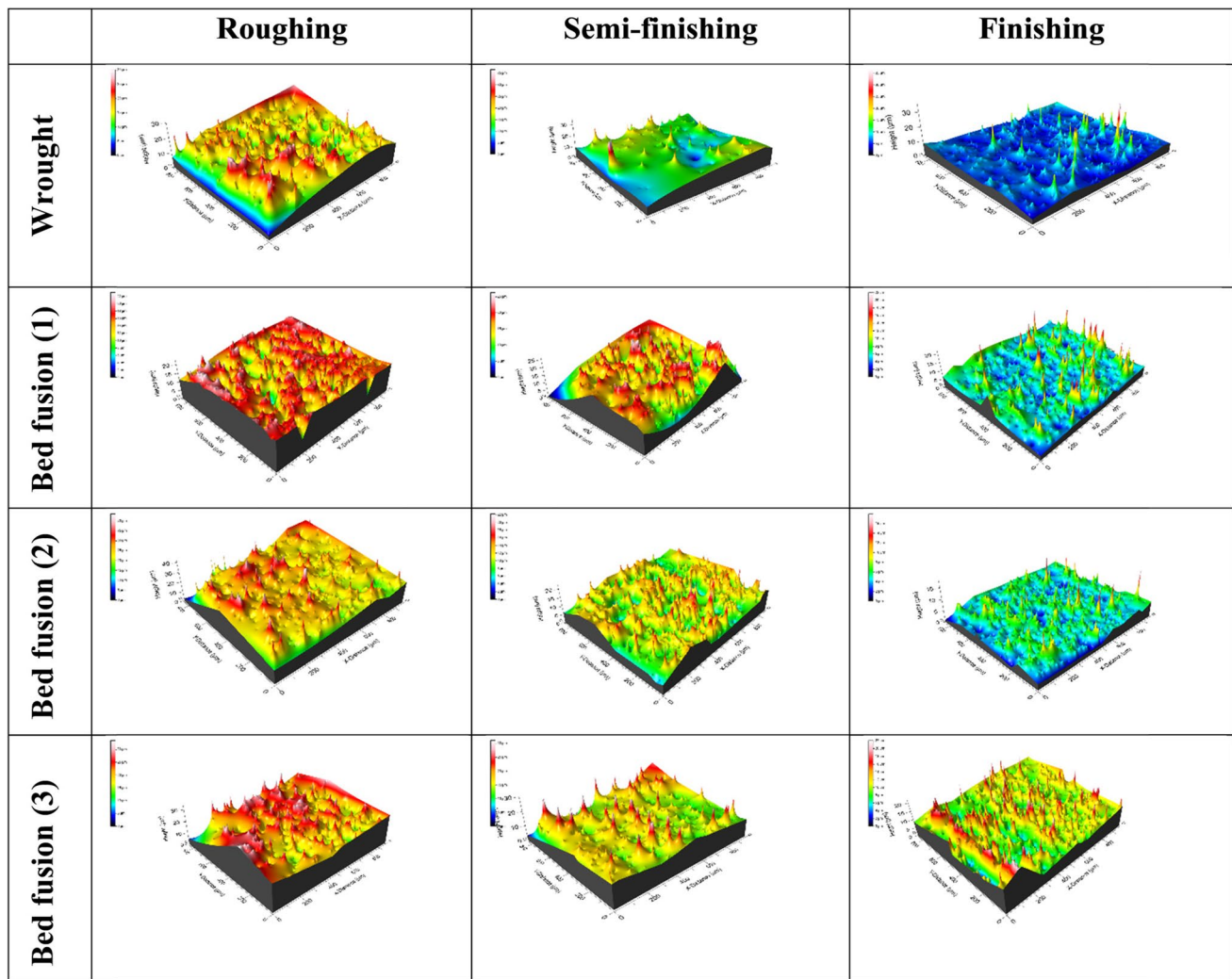


Fig. 9 3D average surface roughness of wrought and LPBF-IN718 samples for rough, semi-finish, and finish cut

performance of monocrystalline Si has been studied [39], discussing variations of WEDM performance (MRR and roughness) depending on the crystallographic orientation. In this reference study, (100)-oriented Si displayed different MRR and surface roughness with changes in machining direction because of different physical characteristics of the crystal orientations. LPBF-IN718 samples with different microstructural characteristics exhibited differences in WEDM performance regarding grain size, HAGB length per area, and crystallographic orientation.

According to the aforementioned results, the effect of microstructural features of IN718 fabricated by LPBF, such as grain size, amount of grain boundary, and grain orientation, exhibited significant differences in WEDM performance and surface morphology of machined samples. Thus, this study highlighted the importance of considering the crystallographic orientation of LPBF-fabricated samples formed by columnar grains along building directions with

specific grain orientations on its WEDM performance and surface integrity.

4 Conclusion

This study investigated the effect of three different WEDM strategies (rough, semi-finish, and finish cutting) on IN718 samples fabricated by the LPBF process while comparing the results with wrought IN718. While the microstructural aspect of LPBF IN718 samples exhibited differences in grain orientation, this aspect of the study should be evaluated in detail by eliminating the effect of grain boundaries to solely focus on the effect of crystallographic orientation, such as floating zone fabrication of single-crystal IN718 samples. In this study, the WEDM strategies showed a decrease in MRR and surface roughness while increasing cutting speed from rough cutting to finishing cut, as well as displaying

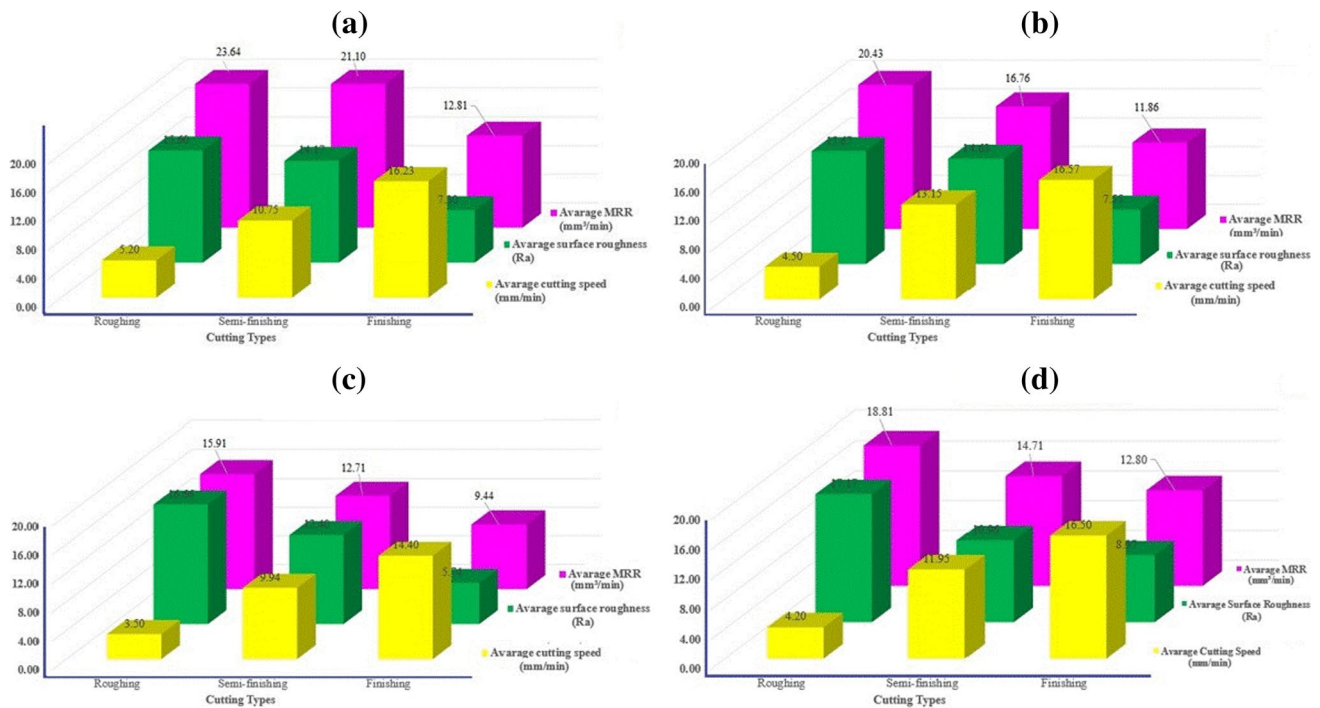


Fig. 10 Average cutting speed, MRR, and surface roughness values of (a) wrought, (b) LPBF-1, (c) LPBF-2, and (d) LPBF-3 IN718 as a result of different WEDM cutting processes

less residue (recast material formed by eroded Cu and Zn from the wire) on the machined surface. Although the effect of machining strategies presented significant differences in surface integrity and machining performance of each IN718 sample, the microstructural differences in wrought and LPBF-IN718 samples showed notable variations in residue formation and surface roughness. The key findings of this study regarding the WEDM performance of LPBF-IN718 can be listed as follows.

1. Less residue (recast material) with a low amount of Cu and Zn was detected on LPBF-IN718 samples compared to wrought-IN718. LPBF-IN718 samples were composed of bigger grains due to epitaxial growth during the LPBF process and thereby contained fewer grain boundaries. However, with the higher area fraction of grain boundary, it is easier to remove the material by WEDM. Thus, LPBF-IN718 with less grain boundary resulted in low MRR but less residue on the surface and lower surface roughness compared to the wrought samples.
2. Machining of LPBF-3 samples resulted in the highest surface roughness ($17.17 \mu\text{m}$) among LPBF-IN718 samples, which was expected due to its high HAGB length per area accelerating erosion of brass-coated Cu wire.
3. Single-crystal LPBF-2 sample exhibited better surface quality ($5.74 \mu\text{m}$ roughness) but low MRR and cutting

speed after machining, which is explained by its unique microstructure having strong crystallographic orientation and big grains resulting in less grain boundary on the IN718 surface.

Author contribution Ozkan Gokcekaya: validation, investigation, visualization, original draft preparation. Ali Günen: conceptualization, investigation, supervision, writing—reviewing and editing. Ferhat Ceritbinmez: methodology, validation, investigation. Abdollah Bahador: Writing—reviewing and editing. Takayoshi Nakano: resources, writing—reviewing and editing. Melik Çetin: resources, writing—reviewing and editing.

Funding Open Access funding provided by Osaka University. This work was supported by a Grants-in-Aid for Scientific Research (grant number JP23H00235) from the Japan Society for the Promotion of Science (JSPS) and CREST-Nanomechanics: Elucidation of macroscale mechanical properties based on understanding nanoscale dynamics of innovative mechanical materials (Grant Number: JPMJCR2194) from the Japan Science and Technology Agency (JST).

Declarations

Ethics approval Not applicable.

Consent to participate Not applicable.

Consent for publication The authors hereby consent to publication of the work in IJAMT.

Competing interests The authors declare no competing interests.

Open Access This article is licensed under a Creative Commons Attribution 4.0 International License, which permits use, sharing, adaptation, distribution and reproduction in any medium or format, as long as you give appropriate credit to the original author(s) and the source, provide a link to the Creative Commons licence, and indicate if changes were made. The images or other third party material in this article are included in the article's Creative Commons licence, unless indicated otherwise in a credit line to the material. If material is not included in the article's Creative Commons licence and your intended use is not permitted by statutory regulation or exceeds the permitted use, you will need to obtain permission directly from the copyright holder. To view a copy of this licence, visit <http://creativecommons.org/licenses/by/4.0/>.

References

1. DebRoy T, Wei HL, Zuback JS, Mukherjee T, Elmer JW, Milewski JO, Beese AM, Wilson-Heid A, De A, Zhang W (2018) Additive manufacturing of metallic components – process, structure and properties. *Prog Mater Sci* 92:112–224. <https://doi.org/10.1016/j.pmatsci.2017.10.001>
2. Kuo C-M, Yang Y-T, Bor H-Y, Wei C-N, Tai C-C (2009) Aging effects on the microstructure and creep behavior of Inconel 718 superalloy. *Mater Sci Eng A* 510–511:289–294. <https://doi.org/10.1016/j.msea.2008.04.097>
3. Rubaiee S, Danish M, Gupta MK, Ahmed A, Yahya SM, Yildirim MB, Sarikaya M, Korkmaz ME (2022) Key initiatives to improve the machining characteristics of Inconel-718 alloy: experimental analysis and optimization. *J Mater Res Technol* 21:2704–2720. <https://doi.org/10.1016/j.jmrt.2022.10.060>
4. Ross NS, Srinivasan N, Amutha P, Gupta MK, Korkmaz ME (2022) Thermo-physical, tribological and machining characteristics of Hastelloy C276 under sustainable cooling/lubrication conditions. *J Manuf Process* 80:397–413. <https://doi.org/10.1016/j.jmapro.2022.06.018>
5. Latanision RM (1988) Physical metallurgy of nickel-base alloys as it relates to corrosion. *J Mater Eng* 10:143–162. <https://doi.org/10.1007/BF02833870>
6. Amato KN, Gaytan SM, Murr LE, Martinez E, Shindo PW, Hernandez J, Collins S, Medina F (2012) Microstructures and mechanical behavior of Inconel 718 fabricated by selective laser melting. *Acta Mater* 60:2229–2239. <https://doi.org/10.1016/j.actamat.2011.12.032>
7. Fu Y, Downey ARJ, Yuan L, Zhang T, Pratt A, Balogun Y (2022) Machine learning algorithms for defect detection in metal laser-based additive manufacturing: a review. *J Manuf Process* 75:693–710. <https://doi.org/10.1016/j.jmapro.2021.12.061>
8. Gokcekaya O, Ishimoto T, Hibino S, Yasutomi J, Narushima T, Nakano T (2021) Unique crystallographic texture formation in Inconel 718 by laser powder bed fusion and its effect on mechanical anisotropy. *Acta Mater* 212:116876. <https://doi.org/10.1016/j.actamat.2021.116876>
9. Gokcekaya O, Hayashi N, Ishimoto T, Ueda K, Narushima T, Nakano T (2020) Crystallographic orientation control of pure chromium via laser powder bed fusion and improved high temperature oxidation resistance. *Addit Manuf* 36:101624. <https://doi.org/10.1016/j.addma.2020.101624>
10. Herzog D, Seyda V, Wycisk E, Emmelmann C (2016) Additive manufacturing of metals. *Acta Mater* 117:371–392. <https://doi.org/10.1016/j.actamat.2016.07.019>
11. Narasimharaju SR, Zeng W, See TL, Zhu Z, Scott P, Jiang X, Lou S (2022) A comprehensive review on laser powder bed fusion of steels: processing, microstructure, defects and control methods, mechanical properties, current challenges and future trends. *J Manuf Process* 75:375–414. <https://doi.org/10.1016/j.jmapro.2021.12.033>
12. Zhang L, Li Y, Zhu H (2022) Prediction and optimization of dimensional accuracy of inclined structures fabricated by laser powder bed fusion. *J Manuf Process* 81:281–289. <https://doi.org/10.1016/j.jmapro.2022.06.078>
13. Nain SS, Garg D, Kumar S (2018) Performance evaluation of the WEDM process of aeronautics super alloy. *Mater Manuf Process* 33:1793–1808. <https://doi.org/10.1080/10426914.2018.1476761>
14. Mouralova K, Benes L, Zahradnicek R, Bednar J, Hrabec P, Prokes T, Hrdy R (2019) Analysis of cut orientation through half-finished product using WEDM. *Mater Manuf Process* 34:70–82. <https://doi.org/10.1080/10426914.2018.1544714>
15. Mouralova K, Benes L, Prokes T, Bednar J, Zahradnicek R, Fries J (2020) Machining of pure molybdenum using WEDM. *Measurement* 163:108010. <https://doi.org/10.1016/j.measurement.2020.108010>
16. Ming W, Xie Z, Ma J, Du J, Zhang G, Cao C, Zhang Y (2021) Critical review on sustainable techniques in electrical discharge machining. *J Manuf Process* 72:375–399. <https://doi.org/10.1016/j.jmapro.2021.10.035>
17. Baldin V, Baldin CRB, Machado AR, Amorim FL (2020) Machining of Inconel 718 with a defined geometry tool or by electrical discharge machining. *J Brazilian Soc Mech Sci Eng* 42:265. <https://doi.org/10.1007/s40430-020-02358-7>
18. Kunieda M, Lauwers B, Rajurkar KP, Schumacher BM (2005) Advancing EDM through fundamental insight into the process. *CIRP Ann* 54:64–87. [https://doi.org/10.1016/S0007-8506\(07\)60020-1](https://doi.org/10.1016/S0007-8506(07)60020-1)
19. Polzer A, Mouralova K, Benes L, Zahradnicek R, Fries J (2022) Comparison of machinability of nickel alloys using WEDM. *Proc Inst Mech Eng Part B J Eng Manuf* 236:1268–1281. <https://doi.org/10.1177/09544054221075876>
20. Mohd Abbas N, Solomon DG, FuadBahari M (2007) A review on current research trends in electrical discharge machining (EDM). *Int J Mach Tools Manuf* 47:1214–1228. <https://doi.org/10.1016/j.ijmactools.2006.08.026>
21. Ahmed A, Tanjilul M, Fardin A, Wong YS, Rahman M, Senthil Kumar A (2018) On the design and application of hybrid electrical discharge and arc machining process for enhancing drilling performance in Inconel 718. *Int J Adv Manuf Technol* 99:1825–1837. <https://doi.org/10.1007/s00170-018-2515-7>
22. Ceritbinmez F, Günen A, Akhtar MA, Patel K, Mukherjee S, Yünlü L, Kanca E (2022) Surface integrity characteristics in wire-EDM of HfTaTiVZr refractory high entropy alloy. *Adv Mater Process Technol* 1–18. <https://doi.org/10.1080/2374068X.2022.2130869>
23. Ramakrishnan R, Karunamoorthy L (2008) Modeling and multi-response optimization of Inconel 718 on machining of CNC WEDM process. *J Mater Process Technol* 207:343–349. <https://doi.org/10.1016/j.jmatprotec.2008.06.040>
24. Dabade UA, Karidkar SS (2016) Analysis of response variables in WEDM of Inconel 718 using Taguchi technique. *Procedia CIRP* 41:886–891. <https://doi.org/10.1016/j.procir.2016.01.026>
25. Thejasree P, Binoj JS, Krishnamachary PC, Manikandan N, Palanisamy D (2021) Experimental analysis on wire electrical discharge machining of Inconel 718 using Taguchi's method BT - advances in industrial automation and smart manufacturing, in: A. Arockiarajan, M. Duraiselvam, R. Raju (Eds.), Springer Singapore, Singapore, pp. 497–504
26. Dhale SR, Deshmukh BB (2023) WEDM with different diameter wire electrodes on Inconel 718: improved dimensional deviation, wire consumption and surface quality. *Mater Today Proc* 72:896–903. <https://doi.org/10.1016/j.matpr.2022.09.088>

27. AltınKarataş M (2022) Wire EDM cutting of Inconel 718 nickel-based superalloy: kerf and MRR analysis. *Multidiscip Model Mater Struct* 18:653–672. <https://doi.org/10.1108/MMMS-05-2022-0080>
28. Wei HL, Mazumder J, DebRoy T (2015) Evolution of solidification texture during additive manufacturing. *Sci Rep* 5:16446. <https://doi.org/10.1038/srep16446>
29. Ishimoto T, Hagihara K, Hisamoto K, Sun S-H, Nakano T (2017) Crystallographic texture control of beta-type Ti–15Mo–5Zr–3Al alloy by selective laser melting for the development of novel implants with a biocompatible low Young's modulus. *Scr Mater* 132:34–38. <https://doi.org/10.1016/j.scriptamat.2016.12.038>
30. Hibino S, Todo T, Ishimoto T, Gokcekaya O, Koizumi Y, Iga-shira K, Nakano T (2021) Control of crystallographic texture and mechanical properties of Hastelloy-X via laser powder bed fusion. *Crystals* 11:1064. <https://doi.org/10.3390/cryst11091064>
31. Kieren-Ehshes S, Böhme L, Morales-Rivas L, Lösch J, Kirsch B, Kerscher E, Kopnarski M, Aurich JC (2021) The influence of the crystallographic orientation when micro machining commercially pure titanium: a size effect. *Precis Eng* 72:158–171. <https://doi.org/10.1016/j.precisioneng.2021.04.007>
32. Gokcekaya O, Ishimoto T, Todo T, Wang P, Nakano T (2021) Influence of powder characteristics on densification via crystallographic texture formation: pure tungsten prepared by laser powder bed fusion. *Addit Manuf Lett* 1:100016. <https://doi.org/10.1016/j.addlet.2021.100016>
33. Ceritbinmez F (2021) An investigation on cutting of the cold work steel X153CrMoV12 by WEDM. *Aircr Eng Aerosp Technol* 93:1674–1680. <https://doi.org/10.1108/AEAT-01-2021-0028>
34. Günen A, Ceritbinmez F, Patel K, Akhtar MA, Mukherjee S, Kanca E, Karakas MS (2022) WEDM machining of MoNbTaTiZr refractory high entropy alloy. *CIRP J Manuf Sci Technol* 38:547–559. <https://doi.org/10.1016/j.cirpj.2022.05.021>
35. Lane B, Heigel J, Ricker R, Zhirnov I, Khromschenko V, Weaver J, Phan T, Stoudt M, Mekhontsev S, Levine L (2020) Measurements of melt pool geometry and cooling rates of individual laser traces on IN625 bare plates. *Integr Mater Manuf Innov* 9:16–30. <https://doi.org/10.1007/s40192-020-00169-1>
36. Khorasani M, Ghasemi A, Leary M, Cordova L, Sharabian E, Farabi E, Gibson I, Brandt M, Rolfe B (2022) A comprehensive study on melt pool depth in laser-based powder bed fusion of Inconel 718. *Int J Adv Manuf Technol* 120:2345–2362. <https://doi.org/10.1007/s00170-021-08618-7>
37. Wang J, Zhu R, Liu Y, Zhang L (2023) Understanding melt pool characteristics in laser powder bed fusion: an overview of single- and multi-track melt pools for process optimization. *Adv Powder Mater* 2:100137. <https://doi.org/10.1016/j.apmate.2023.100137>
38. Liu Q, Zhang Q, Zhang M, Zhang J (2015) Effects of grain size of AISI 304 on the machining performances in micro electrical discharge machining. *Proc Inst Mech Eng Part B J Eng Manuf* 231:359–366. <https://doi.org/10.1177/0954405415573062>
39. Liu Q, Zhang Q, Zhang M, Zhang J (2015) Effect of crystallographic anisotropy on micro EDM process. *Mater Manuf Process* 30:961–967. <https://doi.org/10.1080/10426914.2014.962660>
40. Bishara H, Lee S, Brink T, Ghidelli M, Dehm G (2021) Understanding grain boundary electrical resistivity in Cu: the effect of boundary structure. *ACS Nano* 15:16607–16615. <https://doi.org/10.1021/acsnano.1c06367>
41. Corona D, Giannini O, Guarino S, Ponticelli GS, Zarcone M (2022) Experimental investigation on the electrical, thermal, and mechanical properties of laser powder bed fused copper alloys. *J Manuf Process* 76:320–334. <https://doi.org/10.1016/j.jmapro.2022.02.023>
42. Bhujangrao T, Veiga F, Suárez A, Iriondo E, Mata FG (2020) High-temperature mechanical properties of IN718 alloy: comparison of additive manufactured and wrought samples. *Crystals* 10. <https://doi.org/10.3390/cryst10080689>
43. Das S, Joshi SN (2020) Estimation of wire strength based on residual stresses induced during wire electric discharge machining. *J Manuf Process* 53:406–419. <https://doi.org/10.1016/j.jmapro.2020.03.015>
44. Rohilla VK, Goyal R, Kumar A, Singla YK, Sharma N (2021) Surface integrity analysis of surfaces of nickel-based alloys machined with distilled water and aluminium powder-mixed dielectric fluid after WEDM. *Int J Adv Manuf Technol* 116:2467–2472. <https://doi.org/10.1007/s00170-021-07610-5>
45. Alam MN, Siddiquee AN, Khan ZA, Khan NZ (2022) A comprehensive review on wire EDM performance evaluation. *Proc Inst Mech Eng Part E J Process Mech Eng* 236:1724–1746. <https://doi.org/10.1177/09544089221074843>
46. Ran R, Wang Y, Zhang Y, Fang F, Xia Y, Zhang W, Yuan G, Wang G (2022) Alleviating segregation and enhancing tensile properties of Inconel 718 superalloy by twin-roll casting and two-stage cold rolling. *J Mater Res Technol* 20:1216–1225. <https://doi.org/10.1016/j.jmrt.2022.07.143>
47. Wang J, Qian R, Yang X, Zhong Y, Shang C (2022) Effect of segregation on the microstructure and properties of a quenching and partitioning steel. *Mater Lett* 325:132815. <https://doi.org/10.1016/j.matlet.2022.132815>
48. Petropoulos GP, Pandazaras CN, Davim JP (2010) Surface texture characterization and evaluation related to machining BT - surface integrity in machining, in: J.P. Davim (Ed.), Springer London, London, pp. 37–66. https://doi.org/10.1007/978-1-84882-874-2_2
49. Alkahlan B, Tabbakh T, Kurdi A, Pramanik A, Basak AK (2023) Formation and characterization of the recast layer formed on Inconel 718 during wire electro discharge machining. *Materials (Basel)* 16. <https://doi.org/10.3390/ma16030930>
50. Lamikiz A, Ukar E, Tabernero I, Martinez S (2011) 5 - Thermal advanced machining processes, in: J.B.T.-M.M.T. Paulo Davim (Ed.), Woodhead Publishing, pp. 335–372. <https://doi.org/10.1533/9780857094940.335>
51. Todo T, Ishimoto T, Gokcekaya O, Oh J, Nakano T (2022) Single crystalline-like crystallographic texture formation of pure tungsten through laser powder bed fusion. *Scr Mater* 206:114252. <https://doi.org/10.1016/j.scriptamat.2021.114252>

Publisher's Note Springer Nature remains neutral with regard to jurisdictional claims in published maps and institutional affiliations.